

# Nanoscale simulations of directional locking

Joel Koplik\*

*Benjamin Levich Institute and Department of Physics  
City College of the City University of New York, New York, NY 10031*

German Drazer†

*Department of Chemical and Biomolecular Engineering  
Johns Hopkins University, Baltimore, MD 21218*

(Dated: September 25, 2018)

## Abstract

When particles suspended in a fluid are driven through a regular lattice of cylindrical obstacles, the particle motion is usually not simply in the direction of the force, and in the high Péclet number limit particle trajectories tend to lock along certain lattice directions. By means of molecular dynamics simulations we show that this effect persists in the presence of molecular diffusion for nanoparticle flows, provided the Péclet number is not too small. We examine the effects of varying particle and obstacle size, the method of forcing, solid roughness, and particle concentration. While we observe trajectory locking in all cases, the *degree* of locking varies with particle size and these flows may have application as a separation technique.

---

\*koplik@sci.cuny.cuny.edu

†drazer@jhu.edu

## I. INTRODUCTION

Macroscopic particles suspended in a fluid and driven through a periodic lattice of solid obstacles tend to move in (commensurate) periodic trajectories. In general, these periodic trajectories are not aligned with the driving force.[1, 2] In fact, the average trajectory angle typically remains locked to a given lattice direction over finite intervals of the forcing angle (*directional locking*). The locking direction  $\alpha$  ( $= \arctan(q/p)$ , where  $(p, q)$  is a lattice direction) and its relation to the forcing angle  $\theta$  depends on the properties of the particles. Therefore, particles of different species driven by the same external force could migrate at different angles with respect to the underlying lattice of solid obstacles. This behavior raises the possibility of using periodic obstacle lattices to provide deterministic and continuous separation of suspended particles. In fact, we have experimentally shown the possibility to separate sedimenting particles by size as they move through an ordered array of cylindrical obstacles created with LEGO<sup>®</sup> pegs on a LEGO<sup>®</sup> board.[2]

Experiments on colloidal particles moving through periodic arrays have shown analogous directional-locking behavior in the near-deterministic limit of large Péclet numbers.[3] Moreover, a separation technique based on the deterministic motion of suspended particles in these periodic devices has been successfully used to fractionate colloidal particles of different size, [3], isolate blood plasma from other blood components [4], separate and label cells [5] as well as to isolate selected cell types for tissue engineering applications.[6] Similar locking behavior is observed in the transport of suspended colloidal particles through spatially periodic, smooth, two-dimensional energy landscapes, arising from an array of optical tweezers.[7] Introducing an optical lattice in a microfluidic channel has also been shown to selectively induce locked-in trajectories that deflect specific particle species in a direction different from the average flow, thus providing a means for lateral fractionation based on the dielectric properties of the particles.[8, 9] An analogous optical fractionation method is based on the presence of locked-trajectories depending on particle size.[10, 11]

Simulations which faithfully incorporate all of the relevant experimental features of colloidal particles – finite particle and obstacle size, accurate hydrodynamics and Brownian motion – are not as yet available. The motion of tracer particles moving through an array of solid obstacles was recently investigated using a Fokker-Planck equation approach, and directional locking was observed at large Péclet numbers.[12] However, these simulations

do not account for particle-solid hydrodynamic interactions or other particle size effects. The case of macroscopic particles was recently investigated by means of Stokesian dynamics simulations, showing that directional locking occurs in the presence of irreversible particle-obstacle interactions.[1] These irreversible forces, on the other hand, are added *ad hoc*, typically to prevent overlap in the Stokesian dynamics simulations. In addition, these simulations correspond to the limit of zero inertia and deterministic motion. Directional locking (or phase-locking) has also been observed in simulations of a number of related transport phenomena, including driven vortex lattices,[13] the motion of overdamped particles in periodic force fields,[14] particles driven through a colloidal lattice,[15] particles moving on crystalline surfaces,[16] and periodic energy landscapes in general.[17] Most of these simulations, however, investigate the motion in an external field and not the interaction of suspended particles with solid obstacles.

In this paper we use molecular dynamics simulations to show that directional locking occurs in the transport of nanoparticles, provided the Péclet number is not too small. These simulations allow us to examine the complex interplay between Brownian motion and different driving fields, together with hydrodynamic interactions (with possible inertia contributions), and other finite size effects such as the atomic-scale roughness of the particles. In addition, molecular dynamics simulations also allow us to investigate the effect that particle-particle interactions have on the separation behavior at different particle concentrations. Moreover, at low concentrations and for certain orientations of the driving force, we show that particles of different size move in different directions.

## II. METHODS

The calculations are based on standard molecular dynamics techniques [18] for atoms interacting via Lennard-Jones (LJ) potentials:

$$V_{\text{LJ}}(r) = 4\epsilon \left[ \left(\frac{r}{\sigma}\right)^{-12} - c_{ij} \left(\frac{r}{\sigma}\right)^{-6} \right], \quad (1)$$

cut off at  $r_c = 2.5\sigma$ . The coefficient  $c_{ij}$  will be used to vary the interaction according to the atomic species  $i$  and  $j$  involved. We have a three component system consisting of a monatomic suspending liquid (L), mobile nearly-spherical particles (P) composed of atoms rigidly held together, and cylindrical obstacles (O) composed of atoms fixed in place. The

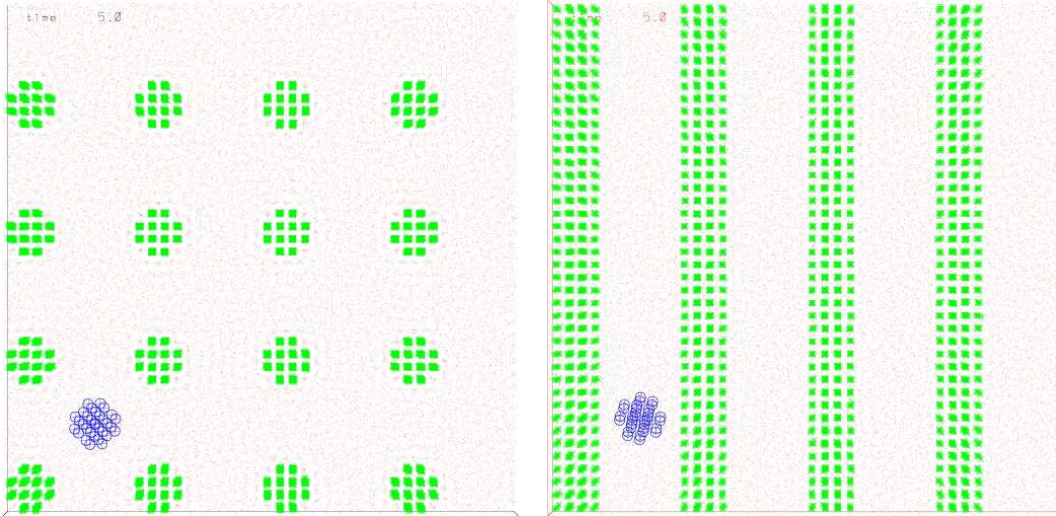


FIG. 1: (Color online) Snapshot of the atomic positions for a simulation involving a  $4 \times 4$  array of cylindrical obstacles of radius 2 (green) and a single mobile sphere (blue), also of radius 2, suspended in a monatomic solvent (red dots). Left:  $x$ - $y$  plane in which the force is applied; right:  $x$ - $z$  plane.

interaction coefficients are chosen to have a “standard” liquid,  $c_{LL} = 1$ , which completely wets both solids,  $c_{LO} = c_{LP} = 1$ , and only a short-distance repulsion between the particles and the obstacles,  $c_{OP} = 0$ . We express all dimensional quantities in terms of the energy scale  $\epsilon$ , the core size  $\sigma$ , and the natural time scale  $\tau \equiv \sigma(m/\epsilon)^{1/2}$ , where  $m$  is the common mass of all atoms. Typical values are  $\epsilon \sim 10^{-21}$  J,  $\sigma \sim 0.3$  nm and  $\tau \sim 2$  ps.

The initial atomic positions form a cubic lattice of density  $\rho = 0.8\sigma^{-3}$ . The particle is defined by selecting all atoms within a prescribed radius of some initial center, while the obstacles are centered on a square lattice in the  $x$ - $y$  plane, and consist of all atoms whose  $(x, y)$  coordinates lie within a second prescribed radius of one of the centers. An example of the atomic positions after equilibration is given in Fig. 1, showing two orthogonal views of a  $4 \times 4$  lattice of cylindrical obstacles of radius 2, along with a particle of radius 2. The simulated region is a cube  $43.09\sigma$  on a side, containing 56,288 solvent atoms, 16 obstacles with 480 atoms each, and the mobile sphere contains 32 atoms. Because they are composed of sets of distinct atoms the particle and obstacle automatically have rough surfaces, and we discuss the effects of varying the degree of roughness below. Periodic boundary conditions are applied in all three directions; the spacing between the obstacles must be commensurate

with the size of the simulation box so that the obstacle lattice has the same periodicity, and in the case shown in the figure the ratio is 1/4. Although the particle could fully sample the periodic geometry in a smaller simulation involving just one unit cell of the obstacle lattice, the larger system provides a larger separation between the particle and its periodic images and the particle’s motion is correspondingly less influenced by the “wake” of the images.

The motion of the atoms follows the Newtonian equations appropriate to each species. Each fluid atom accelerates according to the force exerted by *all* other atoms within interaction range. The particle moves rigidly, so that its center of mass translates under the sum of the LJ forces applied to its individual atoms and rotates in response to the sum of the torques on the individual atoms about the center of mass. The orientation of the particle and its rotational motion is conveniently described by the Euler equations expressed in terms of quaternion variables.[19] The atoms in the obstacles are simply fixed in place. The particle is driven through the obstacle array by adding an external force to its LJ interactions in a prescribed direction in the  $x$ - $y$  plane, or alternatively such a force is applied to each suspending fluid atom to produce a pressure driven flow in the solvent in which the particle is advected.

During the simulation the temperature of the solvent liquid is maintained at  $T = 1.0\epsilon/k_B$  by a Nosé-Hoover thermostat. In principle, the atoms in the particle and obstacle should also have thermal fluctuations about their rigid-lattice positions, but the displacements in a solid are small and this complication has been omitted in most cases. Allowing thermal motion of the obstacle atoms presents little computational difficulty, and can be accomplished by using a stiff linear spring to tether these atoms to their initial lattice sites and allowing them to move in response to the LJ interactions with other nearby atoms. We have added such thermal motion to the obstacles in a few test cases and, outside of an interesting special situation discussed below, we do not observe any significant change in the particle motion. Adding thermal motion to the atoms of the mobile particle is more difficult because the particle’s moment of inertia would vary in time and complicate the solution of the Euler equations.

In these calculations the directed motion of the particle is modified by the Brownian motion resulting from its interaction with the suspending fluid atoms, and the competition may be quantified by the Péclet number. Normally one defines  $Pe = Ua/D_m$  where  $U$ ,  $a$  and  $D_m$  are the average velocity, radius and molecular diffusivity of the particle, respectively, but

this form is awkward here because the velocity is a result of the simulation and measuring the diffusivity in this geometry would require extensive additional simulations. (The motion in  $z$  is diffusive, but the diffusion coefficient is modified from that in pure fluid by the interaction with the rough obstacles.) However, a simpler characterization is possible if we assume that a simple linear drag law applies,  $\mathbf{U} = \gamma\mathbf{F}$ , and that the drag coefficient satisfies the Stokes-Einstein relation  $D_m = k_B T / \gamma$ , in which case  $\text{Pe} = Fa / k_B T$ . In fact, as we shall see below,  $\gamma$  depends on the orientation of  $\mathbf{F}$  with respect to the obstacle lattice so this argument is only approximate, and the latter form for  $\text{Pe}$  is just a convenient parametrization.

### III. RESULTS

We begin with simulations of the system shown in Fig. 1, applying a force

$$\mathbf{F} = (F_0 \cos \theta, F_0 \sin \theta, 0) \quad (2)$$

to the particle. The position of the particle's center of mass is recorded at  $1\tau$  intervals, and the subsequent analysis is based on the  $x$  and  $y$  components of these trajectories. Because of the symmetry of the square obstacle lattice, it suffices to consider forcing angles  $\theta$  between  $0$  and  $45^\circ$ .

#### A. Local behavior

The effects of molecular diffusion are illustrated in Fig. 2 which shows a fine-scale view of the initial particle motion at low and high  $F_0$ . As expected, the motion between obstacles tends toward a straight line, and the motion around obstacles follows their shape more closely at larger  $F_0$ ; note that numerically  $\text{Pe} = 2F_0$  here. At larger scales, the shape of the trajectories is quite sensitive to locking phenomena. In Fig. 3 we display sample trajectories at  $F_0 = 100\epsilon/\sigma$  for forcing angles  $\theta = 36, 30, 26$  and  $22^\circ$ , separately for intermediate and long time intervals of about  $500$  and  $5000\tau$ , respectively. When the force direction is close to a locking angle of  $45^\circ$  (not shown), the particle follows a straight path with detours around the obstacles, and when the forcing angle  $\theta$  is near zero (not shown) the particle bounces back and forth between two rows of obstacles. These two limiting behaviors persist for angles somewhat larger than  $0^\circ$  and somewhat smaller than  $45^\circ$ , respectively. At intermediate

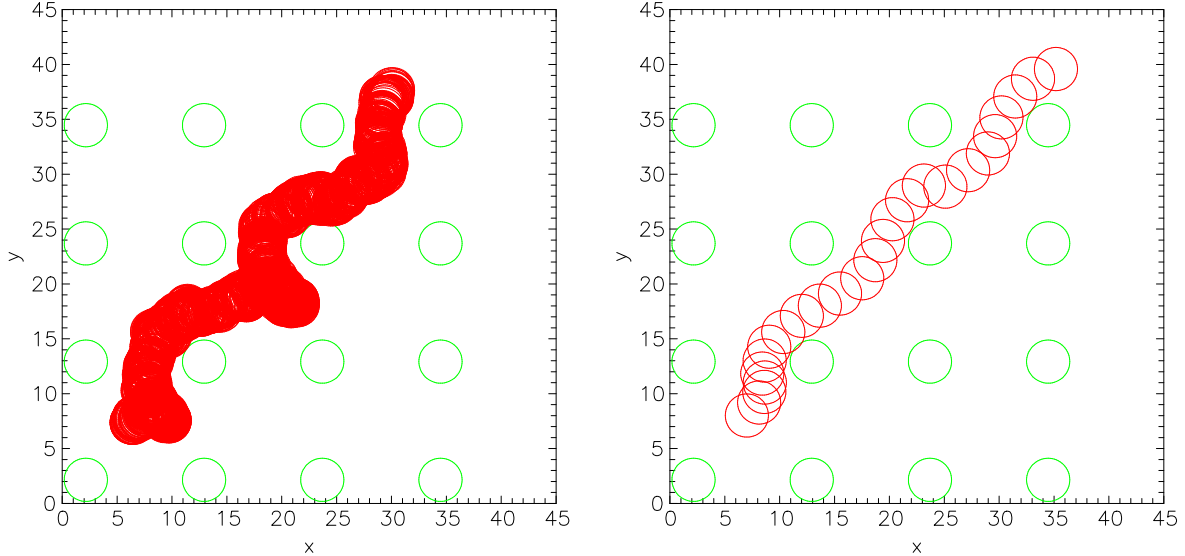


FIG. 2: (Color online) Early stages of the trajectories of a particle forced at  $\theta = 48^\circ$ , shown as a sequence of circles (red) moving through cylindrical obstacles (green). Left:  $F_0 = 5$  until  $2250\tau$ ; Right:  $F_0 = 200$  until  $25\tau$ .

angles in the middle of this interval the motion is rather irregular: segments of variable length along the locking directions at  $45^\circ$ ,  $26.6^\circ$  and  $0^\circ$ . These directions correspond to displacements which would geometrically intersect the obstacle lattice with  $\delta y : \delta x$  of 1:1, 1:2 and 1: $\infty$ ; the other lattice possibilities such as 1:3 or 2:3 do not seem to appear in the trajectories to any significant degree, even when the force is applied at just those values.

At this point we note an important negative result: locking in three-dimensional flows requires cylindrical obstacles which fully obstruct the motion in the third dimension, whereas a cubic array of localized obstacles has no systematic effect on the motion. The reason is that the deflection of the sphere around an obstacle after a close approach should be independent of  $z$  in order for the process to repeat coherently at subsequent obstacles. A cylindrical obstacle has this feature, but if the obstacle is spherical the impact parameter depends on  $z$  and will vary as the particle diffuses in that direction. The direct evidence is given in Fig. 4 which shows the  $x$ - $y$  trajectories of a mobile sphere of radius  $2\sigma$  moving through a cubic array of spheres of the same radius spaced by  $10.77\sigma$ . A force given by Eq.2 is applied with  $F_0 = 50 \epsilon/\sigma$  at forcing angles  $\theta = (22.5, 24.75, 27, 29.25, 31.5)$  and the inclination of the resulting trajectories is essentially the same:  $\alpha = (22.27, 24.51, 27.08, 29.19, 31.52)$ . In this case a single realization at each angle suffices.

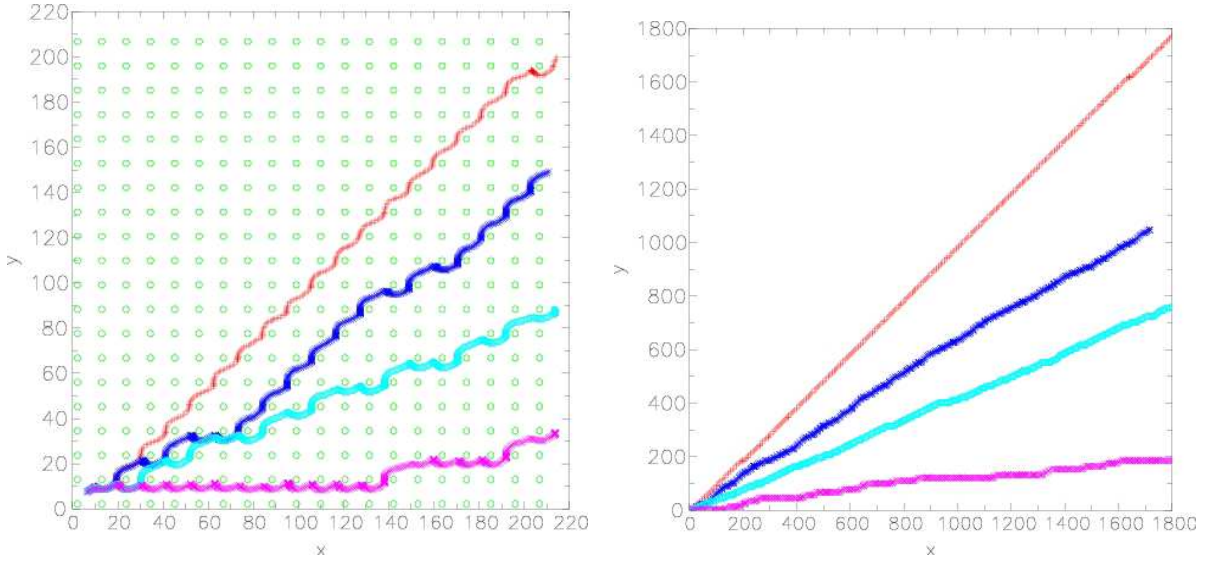


FIG. 3: (Color online) Initial and global trajectories of a particle forced at  $F_0 = 100\epsilon/\sigma$  for angles  $\theta = 36$  (red),  $30$  (blue),  $26$  (cyan) and  $22^\circ$  (magenta), top to bottom.

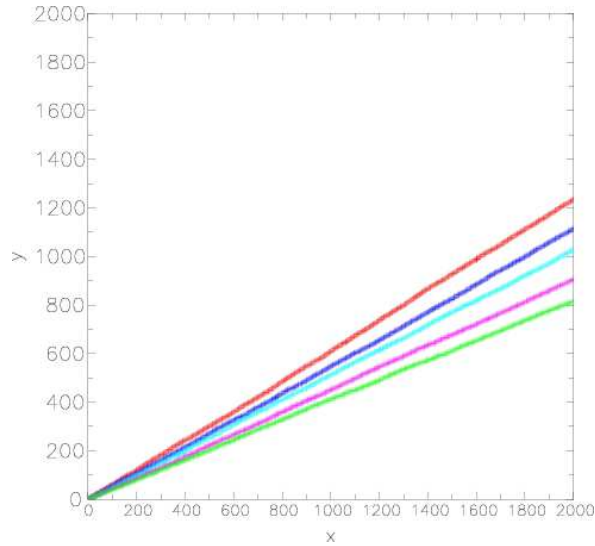


FIG. 4: (Color online) Trajectories of a sphere forced through a three-dimensional cubic array of spherical obstacles, for forcing angles  $\theta = (22.5, 24.75, 27, 29.25, 31.5)$  bottom to top (red, blue, cyan, magenta, green). No locking occurs in this case.

## B. Locking behavior

The locking behavior of the particle motion is determined by the relation between the forcing angle  $\theta$  and the trajectory angle  $\alpha$ , defined as the angle between the end-to-end



vector and the  $x$ -axis. This angle could depend on the length of the trajectory, but in these simulations we observe little sensitivity once the particle covers distances beyond a few hundred  $\sigma$ . The results presented here are based on simulations over a  $5000\tau$  time interval for flows with  $Pe > 100$ , which cover at least this distance. For each case we average over five realizations, obtained by applying a force in the (neutral)  $z$ -direction for different short intervals, to produce a new initial position for the particle. The resulting standard deviation in the mean trajectory angle is one degree or less, and similarly the relative fluctuations in the other quantities discussed below is small. We begin with simulations in the system discussed above, using forces of magnitude  $F_0 = 50, 100$  or  $200\epsilon/\sigma$  oriented at angles  $14$  through  $42^\circ$ . As an alternative to applying a fixed force to the particle which pulls it through the solvent, in a separate series of simulations we apply a pressure gradient to the fluid which drives a flow and advects the particle. In the latter case, a force  $\mathbf{g}$  is applied to each fluid atom at the same set of directions, with magnitude  $g = 0.1, 0.25$  or  $0.5\sigma/\tau^2$ .

The resulting variation of the trajectory angle is shown in Fig. 5, where obvious locking behavior is seen: all of the curves depart significantly from a straight line at  $45^\circ$ . For smaller values of  $\theta$  the trajectory angle is approximately zero in all cases. As expected, the locking behavior is more pronounced at higher forcing values, corresponding to higher  $Pe$ . A more surprising result is that a locking plateau – a range of forcing angles producing the same trajectory angle – appears only at a subset of the possibilities which occur in the ballistic and high  $Pe$  limits,[1, 12] at zero,  $45$  and possibly  $26.6^\circ$ . The latter near-plateau is most evident when the solvent is forced, at the two higher  $g$  values. Presumably the difference arises from molecular diffusion, even for Péclet numbers of several hundred which appear at the highest forcing values here.

When higher values of force are applied to the particle a complication arises: the particle can become jammed into an obstacle and remain there for a variable length of time. The reason for jamming is that both particle and obstacle are rigid solid lattices with (atomic) corners, and if a corner of the mobile particle enters the gap between two layers of the obstacle and the driving force exceeds the typical LJ short-distance repulsive force, an equilibrium may be established. A simple (physically realistic) remedy is to introduce thermal motion for the atoms in the two solids, which alters the force balance and mobilizes the particle. This technique was used in a few test situations at  $F_0 = 200$ , with no significant change in the results, and could be used to reach higher  $Pe$  values, but we have not pursued this

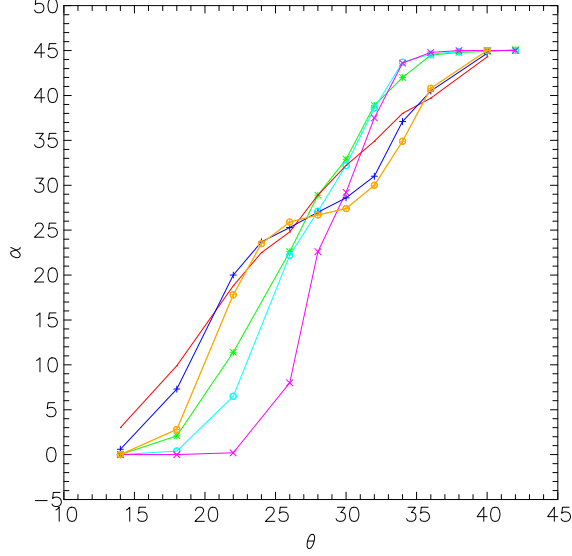


FIG. 5: (Color online) Trajectories angles  $\alpha$  vs. forcing angle  $\theta$  when the particle is driven either by a constant force applied to the particle of magnitude  $F_0 = 50$  (green,\*), 100 (cyan,o) or  $200\epsilon/\sigma$  (magenta,x), or else by an acceleration  $g = 0.1$  (red,·), 0.25 (blue,+), or  $0.5\sigma/\tau^2$  (orange,⊕) applied to the solvent atoms.

extension systematically.

In addition to the angle we measure the average velocity  $V$  in each trajectory, defined as the end-to-end distance in the  $x$ - $y$  plane divided by the elapsed time, and an “excess length”  $\xi$ , defined as the (approximate) path length divided by the end-to-end distance. The path length is approximated by dividing the trajectory into straight segment of duration  $1\tau$  and summing the (two-dimensional) segment displacements, and the significance of  $\xi$  is that it measures the deviation of a trajectory from a straight line and thereby the degree to which an individual trajectory is in fact locked at the angle  $\alpha$ . The value of  $\xi$  of course depends on the time interval of the segments used to measure it and is not unique, but rather is meant to provide a simple measure of “dithering” – deviations from a straight line along a trajectory. The result for the average velocity and excess length are presented in Fig. 6 The velocities are largest and the excess length smallest when the forcing direction is along the  $x$ -axis and the particle simply moves through one row of the lattice, and similar behavior is found when the forcing is close to the  $45^\circ$  locking direction. In the forced-particle cases, the velocity is smallest and the dithering is largest at intermediate forcing angles where the particle trajectory does not follow a single locking angle. The forced-solvent simulations

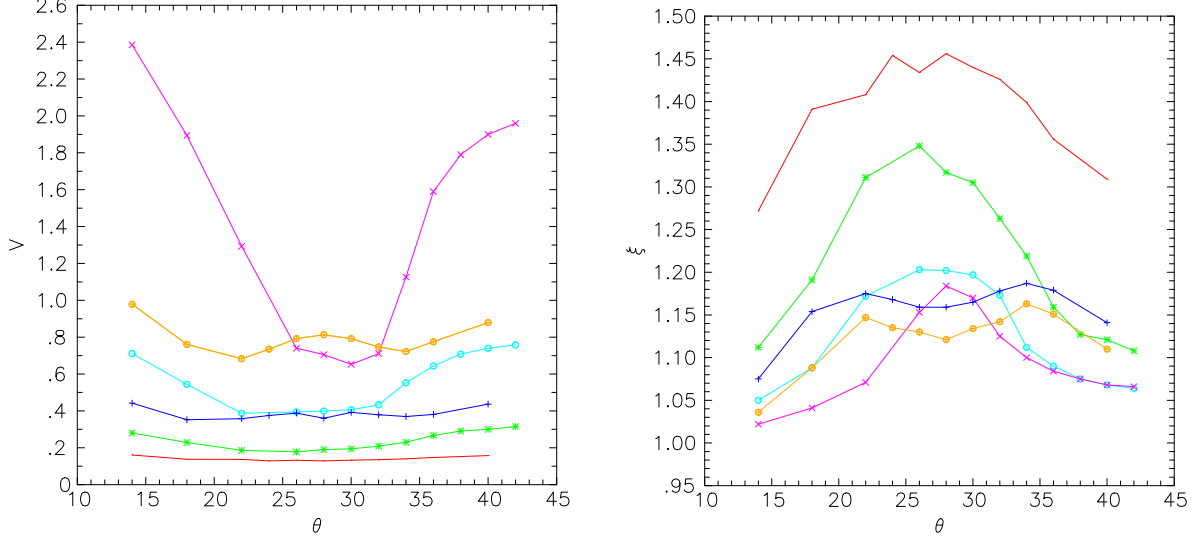


FIG. 6: (Color online) Average velocity (left) and excess length (right) for the trajectories in Fig. 5, plotted with the same colors and symbols.

at  $g = 0.25$  and  $0.5\sigma/\tau^2$  show some evidence for a plateau at the  $26.6^\circ$  locking angle, and correspondingly have local maxima in  $V$  and local minima in  $\xi$ .

Next, we consider the effect of varying the geometry. We compare the behavior of particle of radius 2, 4 and  $5.5\sigma$ , in a lattice of cylinders of the previous radius 2 but a larger spacing  $17.2\sigma$  in order to accommodate the larger particles. A force  $F_0 = 100$  is applied to the particle in each case. In Fig. 7 we show the trajectory angle, average velocity and excess length as a function of forcing angle. In this situation, we again see that the trajectories do not simply follow the force direction, and at least for the two smaller particles the presence of three locking plateaus. In comparison to the previous case, the larger obstacle spacing leads to a  $26.6^\circ$  plateau for particles of radius 2, which suggest that a looser obstacle lattice, or more precisely a larger ratio of obstacle spacing to particle size, may improve locking. The overall velocity decreases with particle size, reflecting the increase in the hydrodynamic drag coefficient with radius, and the variation with angle shows similar trends as in the previous geometry, high velocities and low  $\xi$  near the locking direction at  $45^\circ$  and near  $26.6^\circ$  for the two smaller particle sizes where a locking plateau is present. The radius 4 simulations, which extend into the  $0^\circ$  locking regime, show a velocity maximum and an excess length minimum there, consistent with the previous system, but the other particle cases have not covered this regime.

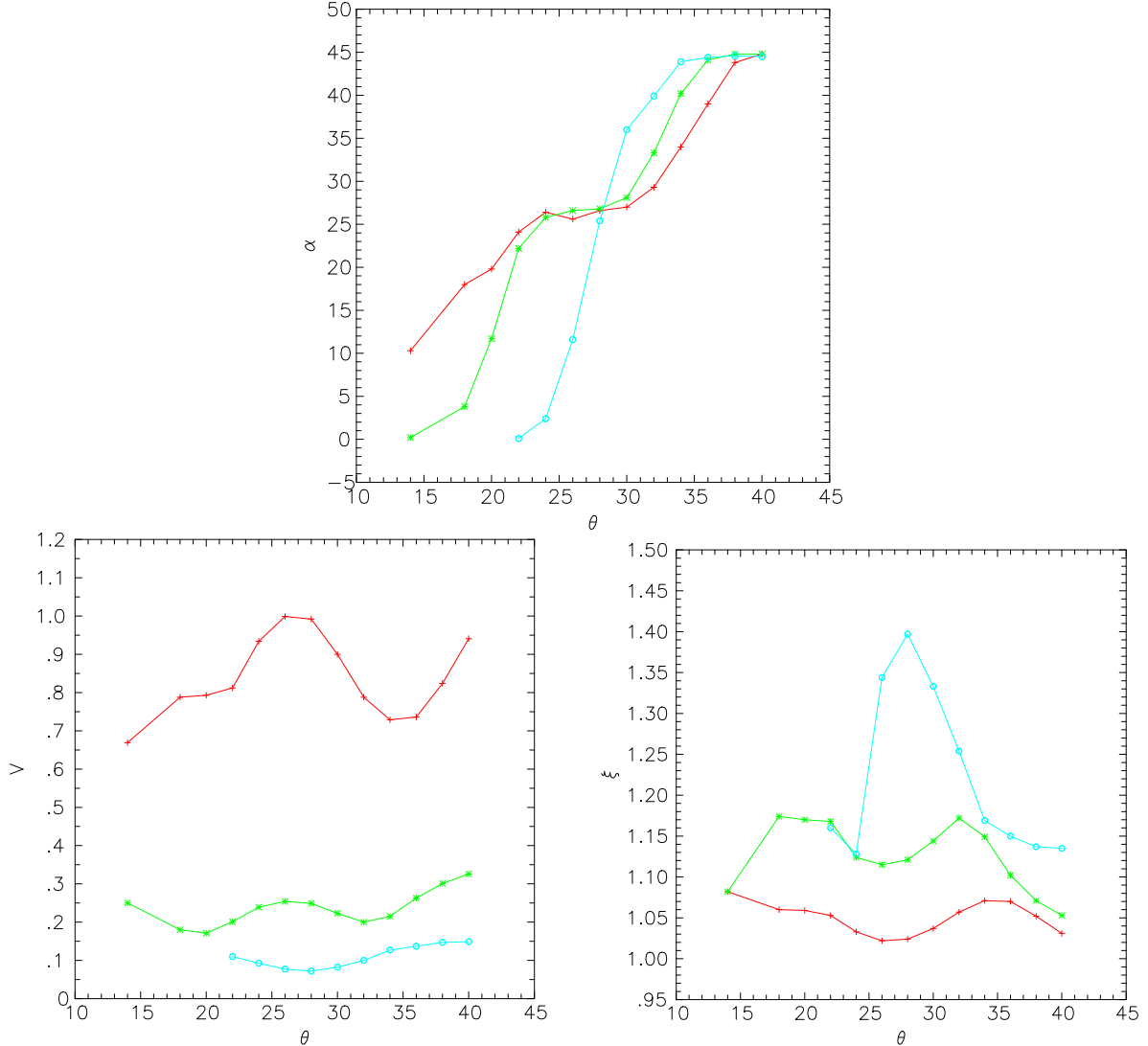


FIG. 7: (Color online) Effects of size. Trajectory angle (top), average velocity (left) and excess length (right) as a function of forcing angle for particles of radius 2 (red,+), 4 (green,\*) and 5.5 (cyan,o) in the larger-spacing obstacle lattice.

We have also varied the particle and obstacle size so as to explore the effects of surface roughness. The scale of the roughness is controlled by the size of the atoms comprising the particle and obstacles, so if we double their radii we have reduced the *relative* roughness by a half. On the other hand, if at the same time we double the obstacle spacing we nominally have scaled the system up in size by a factor of two, and to the extent that these simulations are in the Stokes flow regime (the suspending fluid's viscosity is about  $2m/(\sigma\tau)$  so in these simulations the Reynolds number is  $O(1)$ ), the hydrodynamics is unchanged. In Fig. 8 we

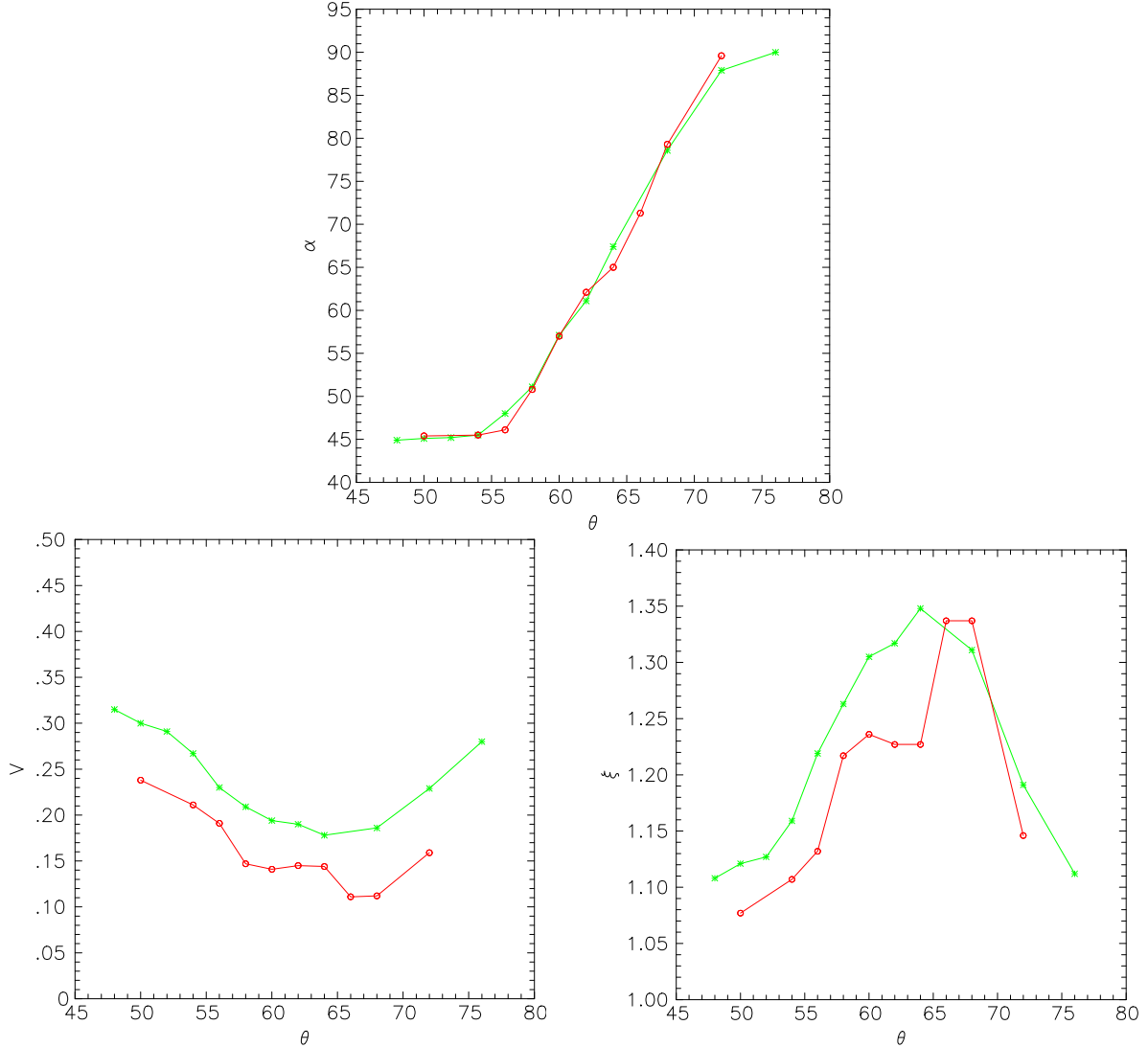


FIG. 8: (Color online) Effects of roughness. Trajectory angle (top), average velocity (left) and excess length (right) as a function of forcing angle for particles and obstacles of radius 2 spaced by 10.77 (green,\*) at force  $F_0 = 50$ , compared to a system doubled in all sizes at force  $F_0 = 100$  (red,o).

compared the results of doubling all sizes and applying a force of magnitude 100 to the original radius 2 case at a force of 50; doubling the particle size approximately doubles the hydrodynamic drag so as to provide a fair comparison. As seen in the figure, there is no significant change in the trajectory angle, and approximate agreement in the velocities and excess length. These results suggest that it is the absolute scale rather than the relative amount of roughness which controls the behavior.

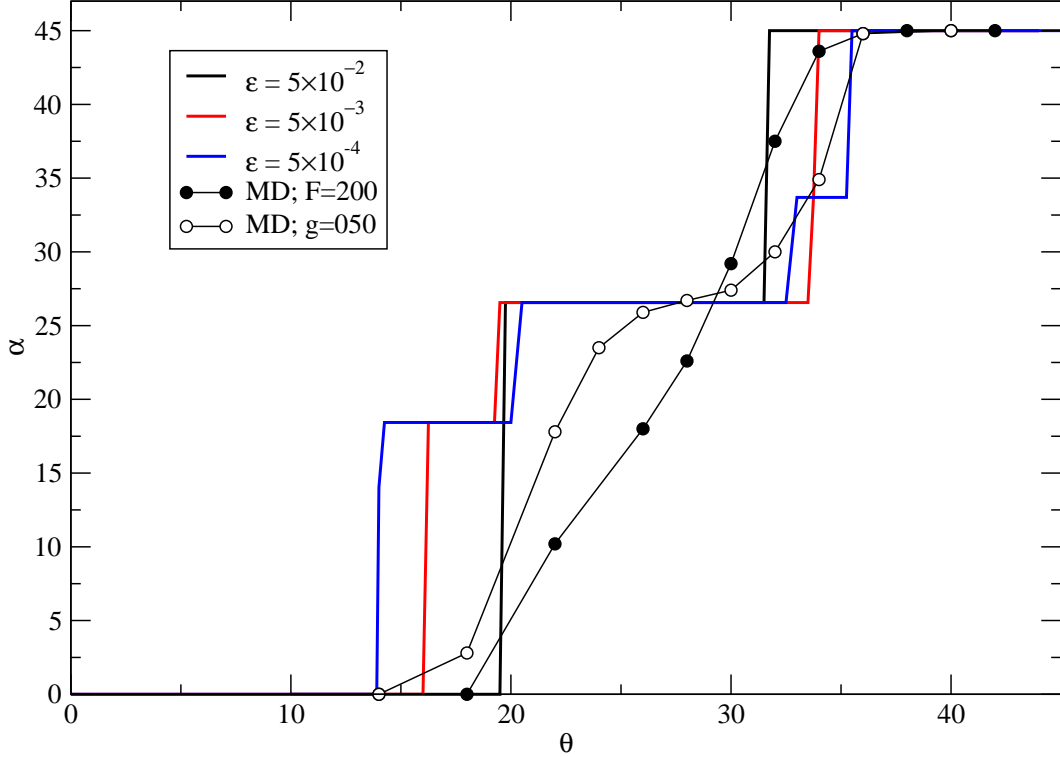


FIG. 9: (Color online) Trajectory angles  $\alpha$  as a function of the forcing direction  $\theta$ . The solid lines correspond to Stokesian dynamics simulations with roughness parameters as indicated. The symbols correspond to the molecular simulations in Fig. 5 for  $F_0 = 200\epsilon/\sigma$  (solid) and  $g = 0.5\sigma/\tau^2$  (open).

### C. Deterministic behavior in the Stokes limit

In previous work we investigated the high Pe limit by means of Stokesian dynamics (SD) simulations, and showed the presence of directional locking.[1] Stokesian dynamics simulations incorporate hydrodynamic interactions between the suspended particles and the solid obstacles in the limit of zero Reynolds number. In addition, a short-range repulsive force is typically introduced in SD simulations to qualitatively model the effect of non-hydrodynamic interactions, such as irreversible forces originating from surface roughness. In fact, the observed locking behavior was shown to depend on a small parameter  $\epsilon$  that determines the range of the repulsive force or the relative magnitude of the surface roughness.

Here, we compare SD simulations with the behavior of nanoparticles at relatively large Péclet numbers. The obstacle lattice in the SD simulations is represented by an array of fixed spheres and the suspended particle moves in the plane of the array (note that in the case of

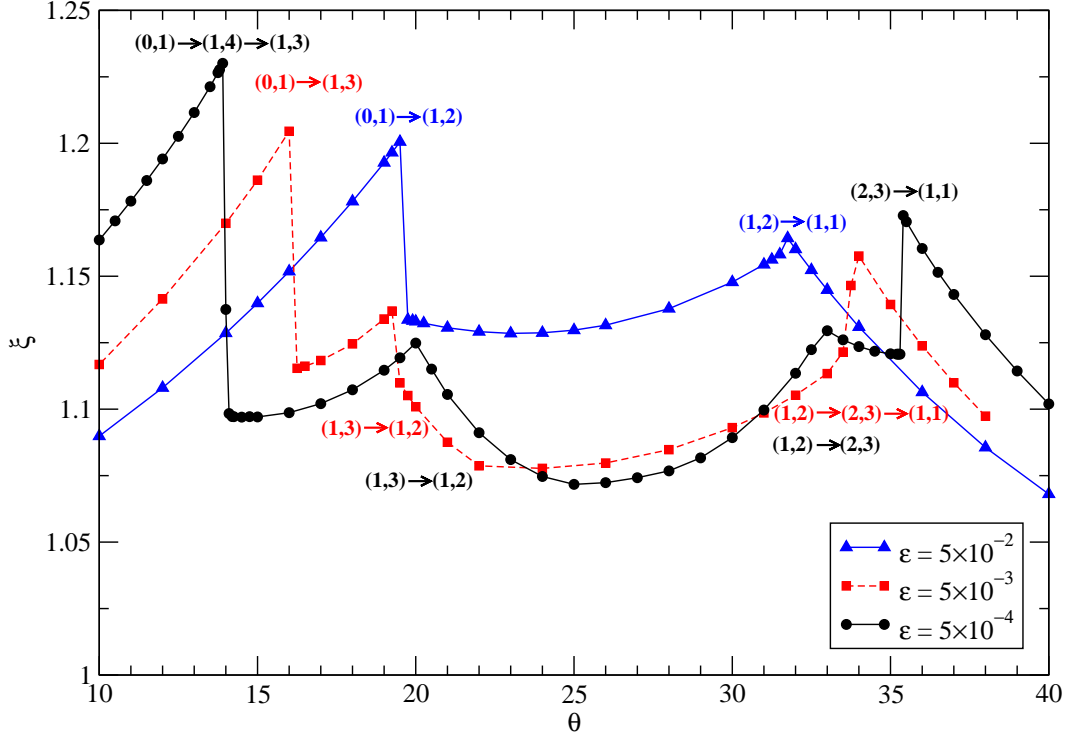


FIG. 10: (Color online) Excess length  $\xi$  as a function of the forcing angle  $\theta$  calculated from Stokesian dynamics simulations for different values of the roughness parameter  $\epsilon$  as indicated. The transitions between locking directions are indicated in the figure, where  $(p, q)$  corresponds to motion at an average angle  $\alpha = \arctan(q/p)$ .

deterministic trajectories we do not have the problem discussed in section III A regarding the absence of locking in the case of spherical obstacles given that the particle does not diffuse in the  $z$  direction). The particles forming the obstacle lattice as well as the moving sphere have the same radius  $a = 1$  and the lattice spacing is  $5a$ , analogous to the system used in the nanoparticles simulations.

The locking behavior is presented in Fig. 9 for different values of the roughness parameter, ranging from  $\epsilon = 5 \times 10^{-4}$  to  $\epsilon = 5 \times 10^{-2}$ . Typically, particles with larger roughness exhibit fewer locking angles, as seen in the figure. We also compare the SD results with the trajectory angles obtained for nanoparticles shown in Fig. 5 for the largest values of the Péclet numbers. We observe that the migration angle of the nanoparticles is closer to the deterministic trajectories corresponding to the largest value of the roughness parameter. It is also clear that the gravity driven nanoparticles exhibit a plateau similar to that observed in the SD simulations for intermediate forcing angles. On the other hand, the

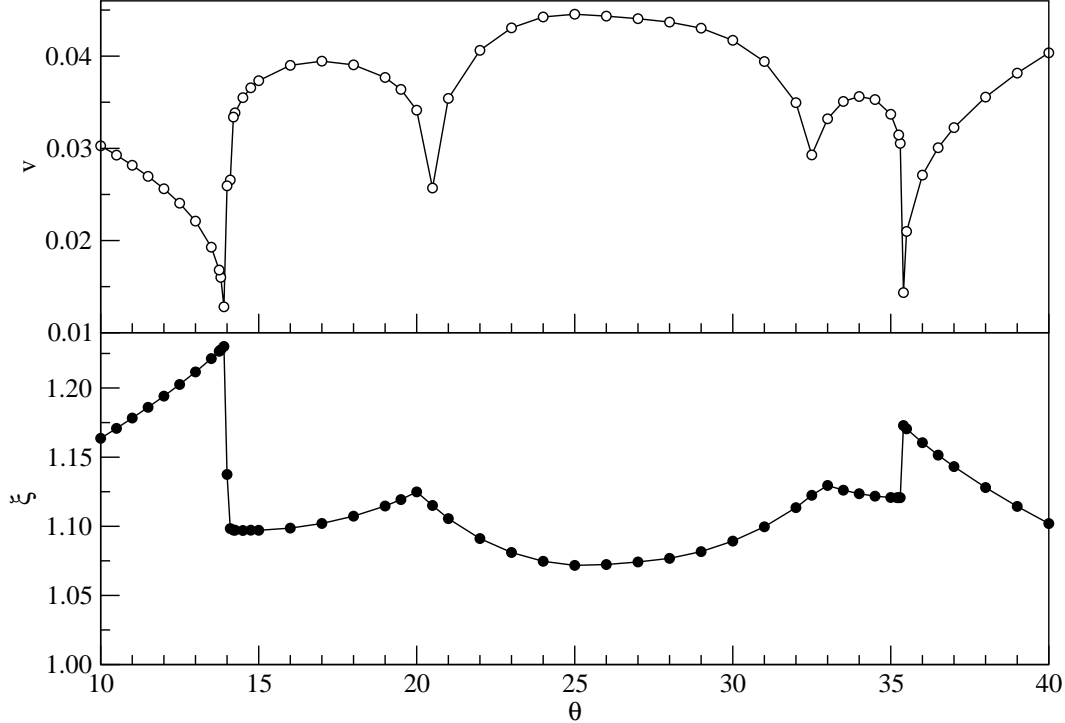


FIG. 11: Average velocity (top) and excess length (bottom) for the trajectories shown in Fig. 10 for the smallest value of the roughness parameter,  $\epsilon = 5 \times 10^{-4}$ .

force-driven nanoparticles seem to transition directly from  $\alpha = 0^\circ$  to  $\alpha = 45^\circ$ . This behavior corresponds to deterministic trajectories with values of the roughness parameter larger than those considered here.

The variation of the excess length measured in the SD simulations is also analogous to the one observed in the case of nanoparticles, but exhibits sharper transitions between locking angles. In Fig. 10 we present the excess length as a function of the driving direction for the different values of the roughness parameter considered in Fig. 9. Similar to what we observe in the transport of nanoparticles at large  $Pe$ , the excess length is smaller when the particles move either at  $\alpha = 0^\circ$  or  $\alpha = 45^\circ$ . At intermediate angles the excess length displays sharp jumps or local maxima at the forcing angles corresponding to transitions between two locking directions. Similar dependence is observed in the motion of nanoparticles presented in Figs. 6 and 7. In the cases in which there is a plateau at intermediate driving angles the excess length displays two clear maxima. On the other hand, in the cases in which  $\alpha = 0^\circ$  and  $45^\circ$  are the only locking directions, there is a single maximum in the excess length around the transition angle.



The deterministic nature of the SD simulations also allowed us to investigate the observed correlation between the average velocity and the excess length in the trajectory of the particles. In Fig. 11 we see that, in fact, they are highly correlated, with local maxima in the excess length corresponding to minima in the average velocity of the suspended particles. In fact, the slowest regions of a given trajectory occur when the particle moves around a solid obstacle with small particle-obstacle separations. On the other hand, the fastest portions of any trajectory are those in which hydrodynamic interactions with the obstacles are small and particles move close to a straight line. As a result, small values of the excess length, which correspond to trajectories closer to a straight line, also indicate faster motion of the particles, and vice versa.

#### D. Suspensions

Given that the trajectories of a single isolated particle in an obstacle array are not collinear with an applied force and may exhibit locking behavior, a natural question is whether this behavior persists in the presence of other mobile particles. The basic argument for locking is based on the behavior of a single particle approaching a single obstacle but multiple particles in general introduce additional interactions which may alter the result. We have therefore repeated the above calculations for *suspensions* of particles. Two cases are considered, both using obstacles of radius 2 spaced by 17.2, a “small” simulation involving a  $3 \times 3$  unit cell containing 20 mobile particles of radius 2 and 20 of radius 3, and a “large” simulation with a  $5 \times 5$  unit cell, 30 particle of radius 2, 30 of radius 3 and 10 of radius 4. The suspensions are fairly dilute, with particle volume fractions of 6.6% and 3.85% for the small and big cases, respectively. In Fig. 12 we show the trajectory angle for each size of particle in the two systems, when a force of magnitude  $F_0 = 100$  is applied. Although the obstacles evidently have an influence on the trajectories, the effect is considerably reduced in comparison to the simulations involving a single mobile particle. The interactions between the particles alter the motion around the obstacles sufficiently to prevent the accumulation of identical individual displacements. On the positive side, there is a clear sensitivity to the particle radius in the “big” case, at lower total concentration, which suggest that using flow through obstacles as a separation technique is viable for sufficiently dilute suspensions.

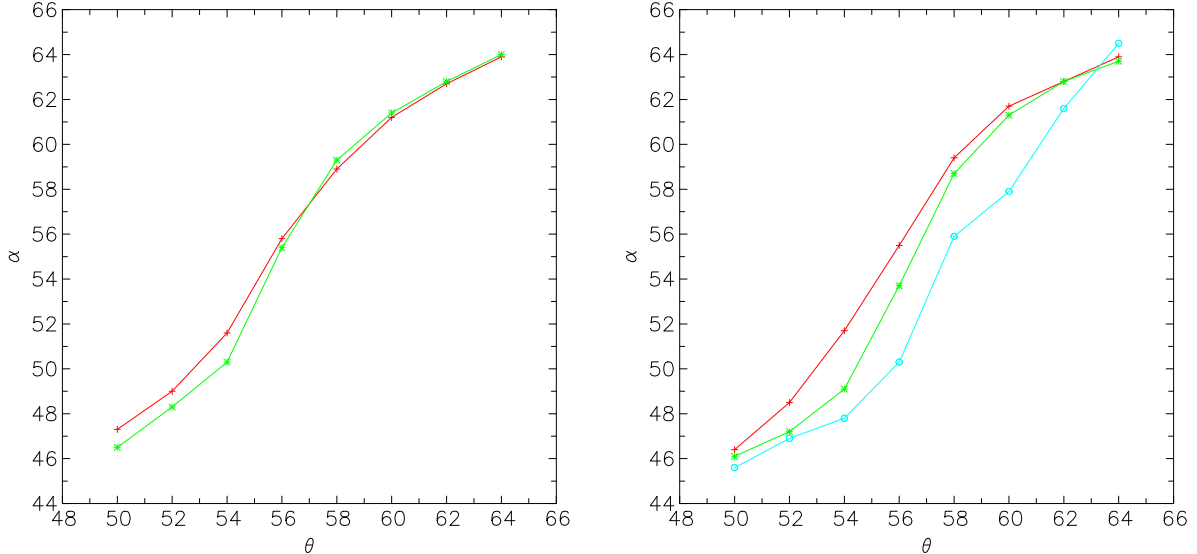


FIG. 12: (Color online) Trajectory angle *vs.* forcing angle for suspensions. Left: “small” and right: “big” suspension, respectively; with radius 2 (red,+0), radius 3 (green,\*) and radius 4 (cyan,o) particles displayed separately.

#### IV. CONCLUSIONS

We have used molecular dynamics simulations to expand the range of previous calculations of locking behavior in flows past obstacle arrays. The new ingredients of the problem considered here are realistic surface roughness, variable particle and obstacle sizes, and a comparison of applying a force directly to the particle with forcing the solvent fluid.

We first considered the behavior of trajectories as a function of Péclet number, and observed that even at  $Pe = 10$  the paths of driven particles resembled those at high  $Pe$ . At general forcing angles, trajectories consisted of segments of variable length aligned along the commensurate locking directions of the obstacle lattice, but near the more robust locking directions ( $45^\circ$  in particular) straighter sinusoidal paths predominated. We also verified the theoretical expectation that cylindrical obstacles are needed to produce locking behavior, by simulating flow through a three-dimensional lattice of spherical obstacles. We then considered the global particle motion for various forcing strengths and orientations and for two types for forcing – driving the particle directly and driving the suspending fluid. The degree of locking was found to increase with  $Pe$  and to be different for the two forcing methods, but for  $Pe = O(100)$  did not show the devil’s staircase plateaus seen in the  $Pe \rightarrow \infty$

limit. These results were compared in detail to those of Stokesian dynamics calculations. Examination of the behavior of particles of different size in the same obstacle lattice suggests that smaller particles may lock more effectively. A follow-up study of the motion of multi-particle suspensions through obstacles verified that the trajectory angles depend on particle size and implies that these may be used as a separation device. Lastly, we considered larger particles and obstacles made of more atoms, which leaves the absolute scale of the roughness (roughly one atom) unchanged but reduces its scale relative to the particle size, and found no significant variation.

The general result is that independent of these variations, the simulations *all* show trajectory locking, in the sense that the average orientation of the trajectory differs from the direction in which the force is applied. Clear effects are seen for all sizes and both forcing mechanisms, once the Péclet number is  $O(10)$  or more. However, the sharp step-wise transitions which occur in the absence of Brownian motion are smoothed by molecular diffusion and most of the locking angles observed in the convective limit, shown for example in Fig. 9, are not apparent at finite Péclet number. These results are subject to the usual limitation of molecular dynamics calculations: small sizes and short times in comparison to many laboratory studies and to continuum methods which do not track atomic motions, but the simulations nonetheless exhibit Navier-Stokes behavior and provide relevant results. Furthermore, for actual nanoparticle applications the simulations operate directly at the relevant scales.

This material is partially based upon work supported by the National Science Foundation under Grant No. CBET-0731032.

- 
- [1] J Frechette and G Drazer, “Directional locking and deterministic separation in periodic arrays,” *J. Fluid Mech.* **627**, 379 (2009).
  - [2] M. Balvin, E. Sohn, T. Iracki, G. Drazer, and J. Frechette, “Directional locking and the role of irreversible interactions in deterministic hydrodynamics separations in microfluidic devices,” *Phys. Rev. Lett.* **103**, 078301 (2009).
  - [3] Lotien Richard Huang, Edward C Cox, Robert H Austin, and James C Sturm, “Continuous particle separation through deterministic lateral displacement,” *Science* **304**, 987 (2004).

- [4] J. A Davis, D. W Inglis, K. J Morton, D. A Lawrence, L. R Huang, S. Y Chou, J. C Sturm, and R. H Austin, “Deterministic hydrodynamics: Taking blood apart,” *Proc. Natl. Acad. Sci.* **103**, 14779 (2006).
- [5] K. J Morton, K. Louterback, D. W Inglis, O. K Tsui, J. C Sturm, S. Y Chou, and R. H Austin, “Crossing microfluidic streamlines to lyse, label and wash cells,” *Lab chip* **8**, 1448 (2008).
- [6] James V. Green, Milica Radisic, and Shashi K. Murthy, “Deterministic lateral displacement as a means to enrich large cells for tissue engineering,” *Anal. Chem.* **81**, 9178 (Nov. 2009).
- [7] Pamela T. Korda, Michael B. Taylor, and David G. Grier, “Kinetically Locked-In colloidal transport in an array of optical tweezers,” *Phys. Rev. Lett.* **89**, 128301 (2002).
- [8] M. P. MacDonald, G. C. Spalding, and K. Dholakia, “Microfluidic sorting in an optical lattice,” *Nature* **426**, 421 (Nov. 2003).
- [9] K. Dholakia, Woei Ming Lee, L. Paterson, M.P. MacDonald, R. McDonald, I. Andreev, P. Mthunzi, C.T.A. Brown, R.F. Marchington, and A.C. Riches, “Optical separation of cells on potential energy landscapes: Enhancement with dielectric tagging,” *IEEE J. Sel. Topics Quantum Electron.* **13**, 1646 (2007).
- [10] K. Ladavac, K. Kasza, and D. G. Grier, “Sorting mesoscopic objects with periodic potential landscapes: Optical fractionation,” *Phys. Rev. E* **70**, 010901 (2004).
- [11] Y. Roichman, V. Wong, and D. G. Grier, “Colloidal transport through optical tweezer arrays,” *Phys. Rev. E* **75**, 011407 (2007).
- [12] John Herrmann, Michael Karweit, and German Drazer, “Separation of suspended particles in microfluidic systems by directional locking in periodic fields,” *Phys. Rev. E* **79**, 061404 (2009).
- [13] C. Reichhardt and F. Nori, “Phase locking, devil’s staircases, farey trees, and arnold tongues in driven vortex lattices with periodic pinning,” *Phys. Rev. Lett.* **82**, 414 (1999).
- [14] M. Pelton, K. Ladavac, and D. G. Grier, “Transport and fractionation in periodic potential-energy landscapes,” *Phys. Rev. E* **70**, 031108 (2004).
- [15] C. Reichhardt and C. J. O Reichhardt, “Directional locking effects and dynamics for particles driven through a colloidal lattice,” *Phys. Rev. E* **69**, 041405 (2004).
- [16] A. M. Lacasta, J. M. Sancho, A. H. Romero, and K. Lindenberg, “Sorting on periodic surfaces,” *Phys. Rev. Lett.* **94**, 160601 (2005).
- [17] A. M Lacasta, M. Khoury, J. M Sancho, and K. Lindenberg, “Sorting of mesoscopic particles

- driven through periodic potential landscapes,” *Mod. Phys. Lett. B* **20**, 1427 (2006).
- [18] M. P. Allen and D. J. Tildesley, *Computer Simulation of Liquids* (Clarendon Press, Oxford, 1987).
- [19] Denis J. Evans and Sohail Murad, “Singularity free algorithm for molecular dynamics simulation of rigid polyatomics,” *Mol. Phys.* **34**, 327 (1977).